Lab on a Chip

PAPER

Pinned films and capillary hysteresis in microfluidic channels

Yihong Liu,[a] David D. Nolte[a] and Laura J. Pyrak-Nolte[abc]

Pinned water films in a microfluidic channel act as elastic membranes under tension that increase capillary pressures while preserving the mechanical work dissipated around capillary pressure-saturation, P_c–S_w, hysteresis cycles. High-resolution two-photon laser micromachining of SU-8 photoresist was used to fabricate wedge-shaped microfluidic channels that included sharp edge features to pin wetting films during drainage. The films were measured using confocal fluorescence microscopy. The tension in the film acts as an elastic tether that shifts the P_c–S_w hysteresis cycle higher in pressure relative to the hysteresis cycle in the same sample when films are not pinned. The film tension is strongly nonlinear as the restoring force decreases with increasing displacement. The contribution of elastic forces to hysteresis has important consequences for pressure and saturation control in microfluidics.

1. Introduction

The hysteresis of saturations and pressures is ubiquitous in all complex pore geometries that support multiple fluid phases.[1–7] A complete understanding of capillary hysteresis in micro-fluidic devices and other porous media containing immiscible fluids remains elusive. One fundamental contribution to hysteresis is known to arise from the difference in advancing and receding contact angles,[8] *i.e.* the angle at which the fluid-fluid interface meets the solid. Another contribution is the presence of films in microfluidic systems. Films thinner than 0.1 μ experience disjoining pressure that weakly alters capillary pressures.[9,10] Disjoining pressure arises from interactions between a thin film and a solid and is the difference between the pressure in a bulk phase and the pressure in the phase adjacent to a surface. Thicker films (> 0.1 microns) or corner fluids (also known as gutter fluids) can have an effect on capillary pressures when the effective radius of curvature of the channel is reduced by the presence of films,[11–14] but this is purely a geometric effect. As shown here, the mechanical contributions of thick-pinned films to capillary pressure and saturation can be large and nonlinear, even in extremely simple pore geometries.

It is well known that defects, surface roughness and chemical surface heterogeneity pin contact lines and cause an elastic force along the interface.[15–17] This elastic force, f, has been para-meterized by De Gennes [15,16] as

$$f = k(u_l - u_m) \tag{1}$$

where u_l is the position of the interface that is not pinned, u_m is the position of the pinned interface and k is the effective spring constant of the contact line. As the distance between the bulk fluid-fluid interface moves farther from the site of pinning, the elastic force increases, similar to the increase in force that occurs by stretching a spring, which defines Hookean behaviour. In this paper, it is shown that, even in an extremely simple geometry, the pinning force on the contact line exhibits strongly non-Hookean elastic behaviour. As the quantity u_l–u_m increases with increasing capillary pressure, the force on the interface decreases. This counterintuitive decrease in force arises from the change in the pinning length of a pinning defect. For a circular defect the spring constant of the contact line, k, is given by[15]

$$k = \frac{\pi \gamma \theta_o^2}{\ln(l/d)} \tag{2}$$

where γ is the fluid-fluid interfacial tension, θ_o is the unperturbed contact angle, l is the long distance cut-off and d is the defect size that causes the pinning. If the defect size $d(u_l)$ is a function of interface displacement u_l, then elastic but non-Hookean beha-viour results. The effect of pinned films on the capillary pressure is examined for simple wedged-shape micro-fluidic devices that were fabricated to have sharp edges to pin films (Fig. 1). The decrease in the spring constant of the contact line during drainage (and conversely, the increase in k with imbibition) is attributed to a change in the size of the pinning defect.

2. Experimental set-up

2.1 Fabrication procedure

Single SU-8 pores were created using a two-photon polymeriza-tion (2PP) technique. Negative SU-8 epoxy (Microchem Corp) is a photoresist composed of a multifunctional glycidyl ether

[a] Department of Physics, Purdue University, 525 Northwestern Avenue, West Lafayette, Indiana, USA. E-mail: ljpn@purdue.edu; Fax: 765 494 0706; Tel: 765 494 3027
[b] Department of Earth & Atmospheric Sciences, Purdue University, West Lafayette, Indiana, USA
[c] School of Civil Engineering, Purdue University, West Lafayette, Indiana, USA
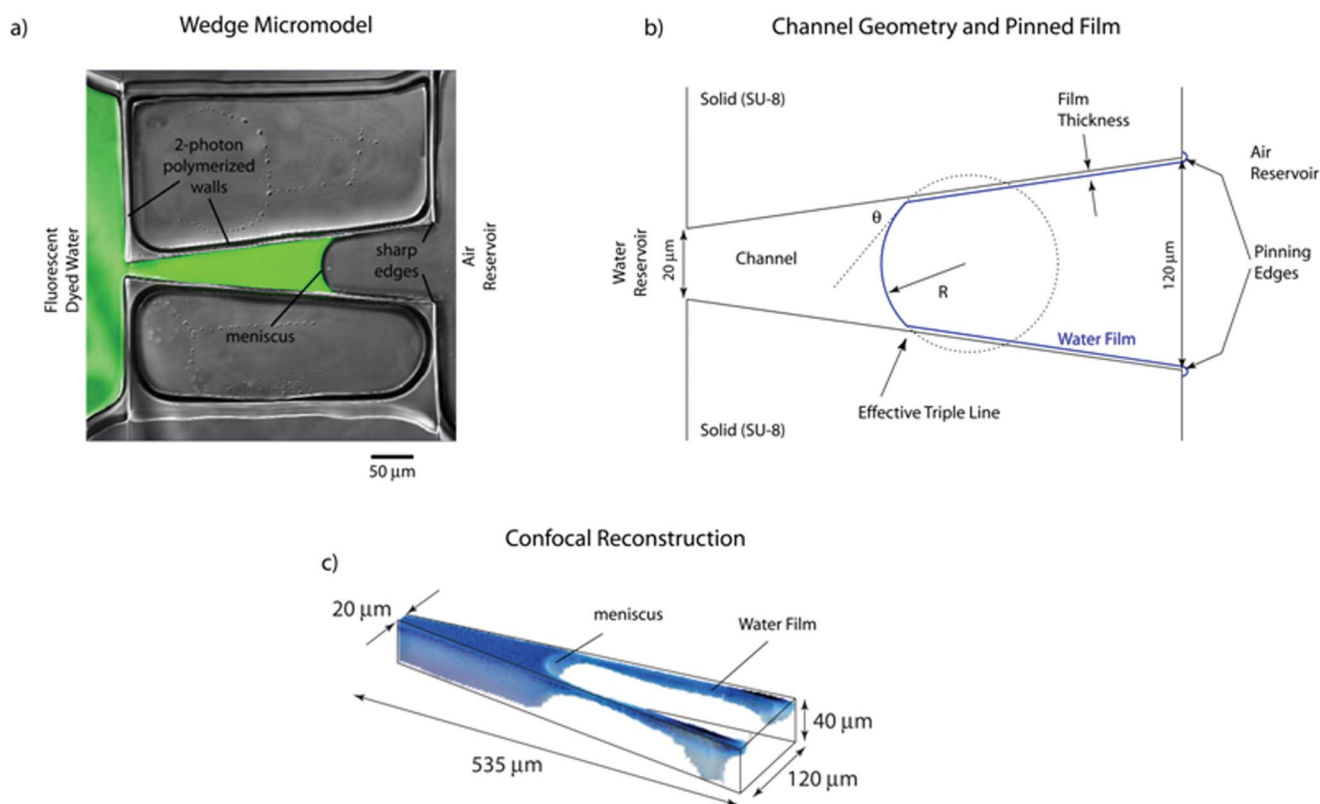
Fig. 1 a) Confocal image of the fabricated wedge-shaped channel showing the geometry of the channel and fluid-fluid interfaces. b) Sketch of the microfluidic channel showing the pinning edges, film (or gutter fluids) and effective contact angle. The channel depth is 40 μm, the small opening to the water reservoir is 20 μm, and the wide opening to the air reservoir is 120 μm. c) Confocal microscopy reconstruction of the fluids and films.

derivative of bisphenol-A novolac from Shell Commercial's EPON SU-8 resin.[18] It is a negative photoresist that remains in place after exposure to UV light and development. Two-photon polymerization is based on two-photon absorption that confines polymerization at the laser focus to a volume on the order of the cube of the wavelength of the laser, and has been used in a variety of applications.[19–23]

To fabricate microfluidic channels, glass cover slips (Corning Square 18 × 18 mm² with a thickness of 190 μm) were used as the substrate for the SU-8 channels. Prior to coating with SU-8, the cover slips were cleaned in an ultrasonic cleaner (Branson1510) in three steps: (1) in deionized water for 5 min, (2) in acetone for 5 min, and (3) in isopropyl alcohol for 5 min. The cover slips were dried with nitrogen at 138 kPa. The top and bottom cover slips were coated with 5 μm thick SU-8 layers to completely encase the micro channel by the photoresist SU-8 to provide a homogeneous surface chemistry. These coated cover slips were pre-baked, and then broad-area exposure was performed with UV light to photopolymerize the 5 μm thick photoresist layer.

On the lower cover slip, a second layer of SU-8 (SU-8_50 MicroChem) was spun to create a layer with a thickness of 40 microns. After soft-baking (30 min at 95 °C), the two-photon polymerization method [11,19] was used to write the walls of the channels. Following the two-photon exposure, UV broad illumination (25 s) was used to fabricate the 3 × 3 mm inlet and outlet ports, as well as a 900 μm long channel connecting the two ports. After processing, the sample was sealed by soft-

baking on a hot plate at 65 and 95 °C for 1 and 3 min, respectively. The entire micro-model was then exposed to a UV lamp for 10 s and post-baked on a hot plate to crosslink the top layer. The final wedge dimensions are 40 microns high, 535 microns long, and 20 microns wide at the exit (wetting phase reservoir) and 120 microns wide at the entrance (non-wetting phase reservoir) (Fig. 1). A key capability of the laser micromachining is the fabrication of sharp edges at the entrance to the air reservoir which act as pinning defects.

2.2 Displacement experiments

The micro-models were initially saturated with the wetting phase, consisting of water dyed with Alex-Fluor 488 at 1 mg/ 10 ml. Drainage and imbibition scans were performed by increasing and decreasing the non-wetting phase (air) pressures. Imbibition occurs when the non-wetting phase pressure decreases and the wetting phase imbibes into the sample. For drainage, as the non-wetting phase pressure increases, the wetting phase is displaced by the non-wetting phase. During each loop, the air pressure was varied in increments of 70 to 280 Pa per step while the water pressure was held constant. At each pressure step, a laser confocal microscope (Zeiss LSM 710) was used to collect a stack of confocal images over the depth of the channel. The confocal stacks were used to reconstruct the three-dimensional geometry of the fluid-fluid interfaces, fluid-solid interfaces, as well as the film structure. In the confocal images, the transverse resolution is 1.19 μm per pixel with a longitudinal slice spacing of 0.714 μm

per slice. After each pressure increment, at least 5 min elapsed to establish mechanical equilibrium of the interface, and each confocal scan took about 1.5 min to complete for 85 z-scan frames that compose the stack. This same procedure was used for all imbibition and drainage scans. The average capillary number (*i.e.* ratio of viscous forces to surface tension) for these experiments is Ca = 2 × 10^{-9}, which is sufficiently small to preclude dynamic effects during triple-line motion.[24]

To compare the capillary pressure-wetting phase saturation (P_c–S_w) hysteresis with and without films, two types of scanning loops were performed. Capillary pressure, P_c, is defined at equilibrium as the pressure difference between the wetting-phase (water) pressure and the non-wetting-phase (air) pressure. The pressure difference between two fluid phases is balanced by the interfacial tension forces and results in curved interfaces between two immiscible fluids. The wetting phase saturation, S_w, is defined as the ratio of the volume of wetting phase (water in these experiments) to the volume of the channel. First, the micromodel was saturated with the wetting phase to a saturation, S_w, of approximately 0.95 to prevent the wetting phase from contacting the sharp edge. In this case, no film was pinned when the wetting phase was subsequently displaced. Then, the air pressure was increased, (incrementally as described above) until a wetting phase saturation of approximately 0.05 was reached. After the drainage scan, the wetting phase was invaded, incrementally, into the throat until S_w was approximately 0.95 again.

After collecting the drainage and imbibition scans for the system without films, the wetting phase was allowed to break through, past the non-wetting-phase outlet, where the two sharp edges in the fabricated micromodel nucleated a thick film (> 1 micron) during the subsequent drainage, shown in Fig. 1b) and 1c). Films were observed to nucleate whenever the wetting phase passed the corners of the channel (S_w slightly greater than

1.0). The wetting phase was withdrawn to a saturation of 0.03, and was then invaded back into the channel.

3. 3D film visualization

Laser confocal microscopy produced stacks of images for each pressure increment after mechanical equilibrium was established. Fig. 2 shows images from the middle of the stack for several different pressures as indicated by the saturation listed above each image. The sections in the top row are the no-film case, and the sections in the bottom row have pinned films. The films or gutter fluids persist as the air is invaded and withdrawn during drainage and imbibition.

Three-dimensional reconstructions of the confocal data both with and without films were made to determine the extent of the pinned films and are shown in Fig. 3 for drainage and imbibition at two roughly equal water (wetting phase) saturations (∼ 20%). The three-dimensional interface curvature is different between drainage and imbibition (Fig. 3 a & c). The contact angles were extracted from the confocal data both in the *x-y* and *z-y* planes and exhibited hysteresis between imbibition and drainage. The contact angles were extracted from the confocal data acquired 4 min after the pressure step was applied, when the interfaces became stable (stopped moving and the measured pressure was constant). Contact angle hysteresis is defined as $\Delta\theta = \theta_a - \theta_r$, where θ_a is the average advancing contact angle and θ_r is the average receding angle (Table 1). Lui *et al.*[8] showed that the hysteresis in the capillary pressure–saturation relationship for equilibrium conditions for a wedge-shaped channel in a microfluidic device in the case with no films is completely determined by advancing and receding contact angles. In other words, the dissipation caused by the movement of the contact line during imbibition and drainage is captured geometrically by the difference between advancing and receding contact angles.
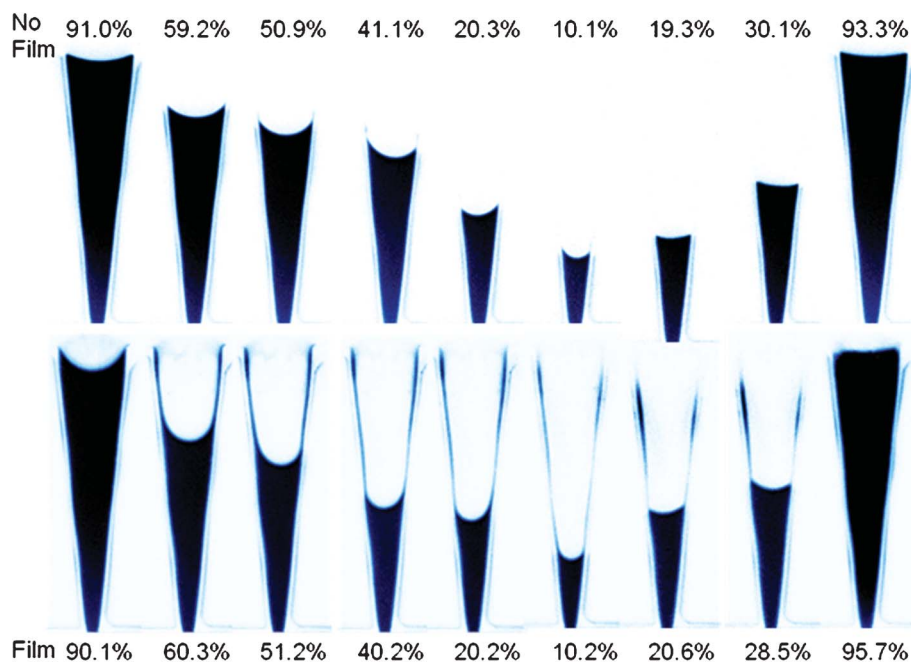

Fig. 2 False-colored mid-stack images show the air (white)—water (blue) distribution within the wedge-shaped channel for different water saturations (given as percentages) for no film (top row) and with film (bottom row). The images start with drainage and end in imbibition.
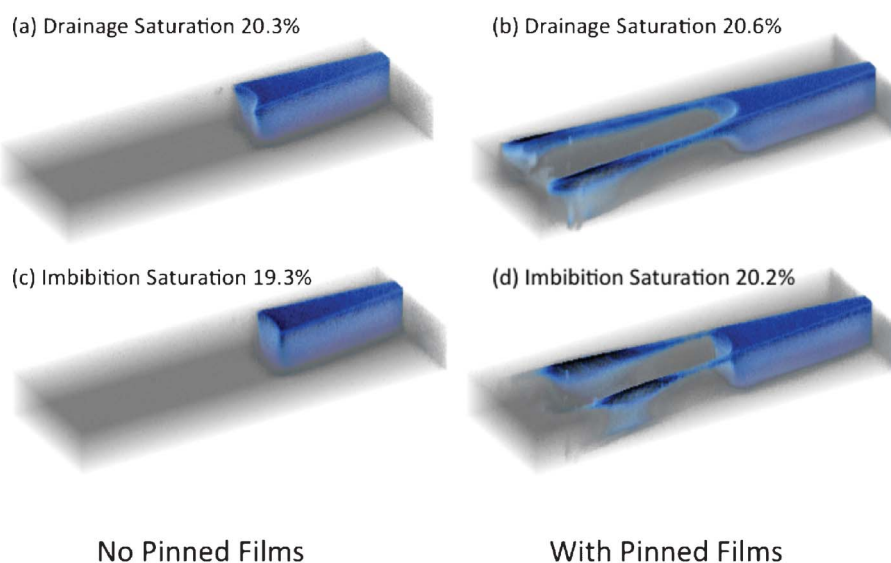
Fig. 3 A three-dimensional visualization of the wetting phase (water) in a wedge-shaped microfluidic channel (sample S7) during drainage (a & b) and imbibition (c & d) showing the location of the films (b & d).

In Fig. 3b & d, the presence of the film, pinned at the sharp vertical edges, is clearly observed, as are the different contact angles at the walls for drainage relative to imbibition. When films are present, the advancing and receding contact angles are smaller than those measured for the film case (Table 1). This arises because the film exerts an additional tension on the interface, and the additional tension is balanced by the reduced contact angle. The films are non-uniform as a consequence of the trapezoidal cross-section area of the channel, with a relatively thick region extending from the meniscus to the pinning edge along the top of the micromodel. The films are not completely resolved by the confocal data (transverse resolution equals 1.19 microns), and films thinner than 30 nm along the vertical walls do not generate sufficient photons to be detected in the confocal photomultiplier tube.

4. Pressure–saturation hysteresis

The capillary pressure–saturation relationships for the wedge-shaped channels with and without films were determined from the externally measured capillary pressure, P_c, and wetting phase saturation, S_w, obtained from image analysis of the confocal stacks at each pressure. A comparison of the P_c–S_w relationship with and without films is shown in Fig. 4 for the two samples S5 and S7. The films contributed less than 1% to the saturation. However, when films were present, the capillary pressure is greater than in the no-film condition. The capillary pressure for

drainage when films were present was larger by ~ 500–1000 Pa for $0.3 < S_w < 0.85$. At lower saturations, the film-induced increase in capillary pressure was smaller and vanished for $S_w < 0.1$. For imbibition, the increase in capillary pressure ranged between 600–900 Pa for $0.2 < S_w < 0.85$.

The additional force required to drain the channel is not attributable to disjoining pressure. The Hamaker constant $(-3.71 \times 10^{-20}$ to -5.06×10^{-20} J) for an air–water-SU8 system, and the 150 nm minimum detectable thickness of the films predict a pressure difference of only 10 Pa, which is negligible relative to the observed difference. Furthermore, as the pressure increase in the channel, the disjoining pressure would increase because of the decrease in film thickness, but this predicts a trend opposite to the trend observed in the results (Fig. 4). Therefore, disjoining pressure cannot explain the observed shift in P_c–S_w curve to higher pressures for the case with films. The Marangoni effect is also not a likely cause, because SU-8 is not soluble in water,[25] and there is no evidence of a gradient in surface tension in the measurements.

The increased capillary pressure in the presence of thick films also cannot be attributed to the reduction in the radius of curvature that occurs in the presence of thick corner films.[11–14,26] From the two-photon approach used in this study, the cross-sectional area of a channel is roughly trapezoidal. Using the approach of ref. 27 but assuming a trapezoidal cross-section with the dimensions of the micro-model, theoretical calculations show that this effect produces an increase in capillary pressure of only $\sim 1\%$ for $S_w < 0.6$ and up to 15% for $0.6 < S_w < 0.9$. This effect is much smaller than the increases observed in the experimental data where the increase in capillary pressure was 25–50% for the same range of saturations (Fig. 4) for both samples. Therefore, the pinned films provide significant elastic forces.

5. Film forces

The film exerts an additional force against the withdrawal of wetting phase during drainage (Fig. 5), and the film likewise

Table 1 Mean values of advancing and receding contact angles, and contact angle hysteresis

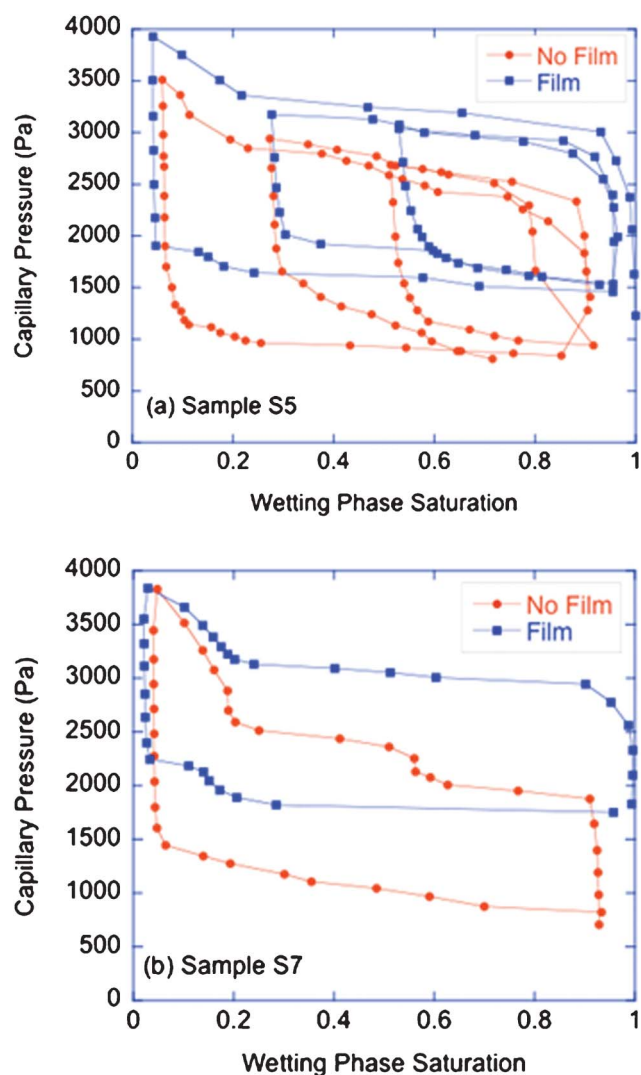|	Drainage (q_r)	Imbibition (q_a)	Hysteresis (D_q)
No Film			
x-y	45°	70°	25°
z-y	70°	87°	17°
Film			
x-y	30°	55°	25°
z-y	50°	70°	20°

Fig. 4 Capillary pressure as a function of wetting phase saturation with (red circles) and without (blue squares) films for samples (a) S5 and (b) S7.

Fig. 5 Sketch of interfacial tension, σ, components for no film (*top*) and when a pinned film is present (*bottom*), illustrating $\Delta\sigma$, the change in interfacial tension, caused by pinned films. The subscripts are: f for film, wn for the wetting-nonwetting interface between the two fluids, ns for the nonwetting phase–solid interface, and ws for the wetting phase–solid interface; τ is the additional tension from the film.

work is equal to the area enclosed by a loop on the pressure–saturation plane. The areas enclosed by the P–S_w loops for the data in Fig. 4 (equal to the mechanical work performed around each loop) were 1.6 nJ with no film and 1.4 nJ with film. There is a consistent 12% smaller hysteresis (work) for the case with films relative to without films, but the difference is small, and the work is nearly equal with and without films. This demonstrates an energy balance in which the films act as an approximately conservative elastic force that shifts the pressure–saturation loops to higher pressures, but do not significantly alter the enclosed work.

The magnitude of the force caused by the films was calculated using

$$F = \Delta P_c * A_{cs} \tag{5}$$

exerts a force that draws in the wetting phase during imbibition. Therefore, the force of the wetting-phase film on the wetting–non-wetting interface is always towards the side of the non-wetting phase. An estimation of the additional tension from the film is calculated from the tension balance. The film tension, or $\Delta\sigma$, during drainage is approximately $0.112\sigma_{wn}$, or 0.0082 N m^{-1}, and during imbibition is $0.126\sigma_{wn}$, or 0.0092 N m^{-1}.

The effect of the films on the curvature of the interface is shown in Fig. 6. The air–water interface for the case without film is compared to the case with film for two midstack images from confocal stacks taken at the same saturation, S_w, of $\sim 51\%$. The interfacial curvatures differ by $\sim 40\%$, in agreement with the shift in capillary pressure in Fig. 4. The contact angle in the case without film is well defined, but in the case with film is clearly much smaller.

The mechanical work expended during imbibition and drainage caused by the irreversible movement of the triple line across the surface is examined to determine if the force exerted on the interface is elastic. The amount of dissipated mechanical
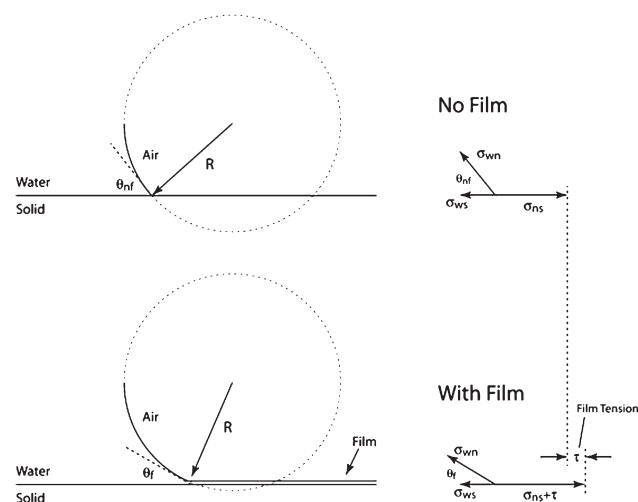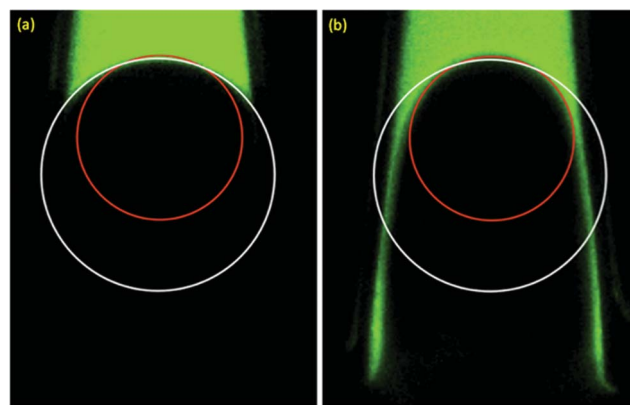

Fig. 6 Mid-confocal stack images show a comparison of the curvature at the same wetting phase saturation of $\sim 51\%$ for sample S7 (a) without film and (b) with film. The white circle indicates the curvature of the water–air interface for the case without film. The red circle indicates the curvature of the water–air interface for the case with film.
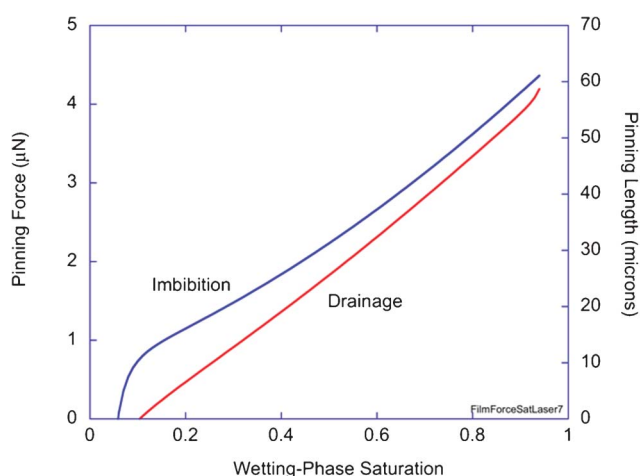
Fig. 7 Calculated pinning force acting on the interface during drainage and imbibition.

where F is the force from the films, ΔP_c is the pressure difference between drainage loops with and without film, and A_{cs} is the cross-sectional area of the channel. The film forces during drainage and imbibition are shown in Fig. 7 as functions of wetting-phase saturation. In each case, the sample was initially saturated with water, then drained and imbibed. The pinning force is the force exerted by the films on the length $d(u_l)$ of the line pinned at the sharp edge. The film force decreases nearly linearly with decreasing wetting phase saturation during drainage (increasing displacement). In the subsequent imbibition, there is almost a step hysteretic increase in the pinning force above the drainage value, followed by an almost linear increase with increasing saturation. This excess force during imbibition leads to positive work performed on the interface that is about 12% larger than drainage, in agreement with the work enclosed by the loop in the hysteresis.

At high saturation, the pinned length (obtained by dividing the pinning force by the surface tension of water in air 0.073 N m^{-1}) is approximately twice the sample height of 40 microns, which is expected for two edges on each side of the non-wetting reservoir. But this pinned length $d(u_l)$ decreases with decreasing saturation as the film is stretched during drainage. Perhaps most remarkable, the pinned length increases again as the water is re-imbibed, which shows that the change in the pinning length is a reversible process.

Energy dissipation, during movement of the triple line, is the origin of hysteresis. The smaller hysteresis for the case with films is because the triple lines of the pinned films do not sweep out as large an area as in the non-pinned case. Hence, the smaller area swept out by the triple line in the case with films leads to smaller hysteresis. The presence of wetting films, which are metastable configurations and might be expected to exhibit irreversible relaxation towards equilibrium, actually reduced the amount of dissipation.

An important aspect is the time it takes for a single experimental hysteresis loop, which is approximately 6 h. The metastable films do not relax significantly in this time frame, which is in agreement with work by Liu et al.[8] who showed that, without films, there was small and extremely slow relaxation of interfaces in the micro-models (1% change in saturation over

5 h). Independent relaxation experiments were performed in the case with films, and although the relaxation was found to be somewhat larger and faster than without films, the relaxation was still small (a change of only 8% in saturation over 5 h). Therefore, the pinning of the triple line, though ultimately metastable, is effectively stable over the time frame of these experiments.

Conclusions

In conclusion, a detailed study of saturation and capillary pressures was performed using confocal microscopy in the case when there is strong pinning of a fluid film in a single channel. The wetting films in these experiments are strongly pinned and in metastable mechanical equilibrium, with negligible relaxation over many hours. A force and energy analysis of the movement of interfaces in the single pore during drainage and imbibition revealed that the wetting films exert an elastic force that is nearly conservative and reversible (within 12%) and shifts the hysteresis loops to higher pressure, but without significantly changing the enclosed hysteresis areas. The nonlinear decrease in the force "constant" with increasing displacement is attributed to restriction of the pinning size $d(u_l)$ with increasing displacement, which must be reversible because of the conservative character of the measured pinning force.

The increase in measured capillary pressure has important consequences for the proper functioning of microfluidic devices with single or multiple channels. The presence of pinned fluids would result in the need for higher pressures to fully saturate channels, especially when the fluids become pinned. In these cases, channel designs should avoid sharp corners that pin fluids. Alternatively, pinning sites can be engineered to help control or maintain interfaces in microfluidic devices, providing a new design component.

References

1 D. Bonn, J. Eggers, J. Indekeu, J. Meunier and E. Rolley, *Rev. Mod. Phys.*, 2009, **81**, 739–805.
2 J. I. Gerhard and B. H. Kueper, *Water Resour. Res.*, 2003, **39**, 1213–1230.
3 S. C. Jose, M. A. Rahman and O. A. Cirpka, *Water Resour. Res.*, 2004, **40**, W12415, DOI: 10.1029/2004WR003363.
4 B. B. Lakshmi, C. J. Patrissi and C. R. Martin, *Chem. Mater.*, 1997, **9**, 2544–2550.
5 W. Linhart, F. Peters, W. Lehmann, K. Schwarz, A. F. Schilling, M. Amling, J. M. Rueger and M. Epple, *J. Biomed. Mater. Res.*, 2001, **54**, 162–171.
6 N. Tsapis, D. Bennett, B. Jackson, D. A. Weitz and D. A. Edwards, *Proc. Natl. Acad. Sci. U. S. A.*, 2002, **99**, 12001–12005.
7 B. Zhao, J. S. Moore and D. J. Beebe, *Science*, 2001, **291**, 1023–1026.
8 Y. Liu, D. D. Nolte and L. J. Pyrak-Nolte, *Water Resources Research*, 2011, **47**, 9.
9 S. Basu and M. M. Sharma, *J. Colloid Interface Sci.*, 1996, **181**, 443–455.

10 B. V. Derjaguin and N. V. Churaev, *J. Colloid Interface Sci.*, 1978, **66**, 389–398.

11 R. P. Mayer and R. A. Stowe, *J. Colloid Sci.*, 1965, **20**, 893–911.

12 P.-E. Oren, S. Bakke and O. J. Arntzen, *SPE Journal*, **1998**, 324–336.

13 H. M. Princen, *J. Colloid Interface Sci.*, 1969, **30**, 359–371.

14 H. Wong, S. Morris and C. J. Radke, *J. Colloid Interface Sci.*, 1992, **148**, 317–336.

15 P. G. De Gennes, *Rev. Mod. Phys.*, 1985, **57**, 827–863.

16 J. F. Joanny and P. G. Degennes, *J. Chem. Phys.*, 1984, **81**, 552–562.

17 G. D. Nadkarni and S. Garoff, *Europhys. Lett.*, 1992, **20**, 523–528.

18 N. LaBianca and J. Gelorme, *Proc. SPIE*, 1995, **2438**, 846–852.

19 S. Maruo, O. Nakamura and S. Kawata, *Opt. Lett.*, 1997, **22**, 132–134.

20 H. B. Sun, S. Matsuo and H. Misawa, *Appl. Phys. Lett.*, 1999, **74**, 786–788.

21 S. Kawata, H. B. Sun, T. Tanaka and K. Takada, *Nature*, 2001, **412**, 697–698.

22 S. Kawata and H. B. Sun, *J. Photopolym. Sci. Technol.*, 2002, **15**, 471–474.

23 Y. Liu, D. D. Nolte and L. J. Pyrak-Nolte, *Appl. Phy. A, Mater. Sci. Process.*, 2010, **100**, 181–191.

24 P. G. De Gennes, F. Brochard-Wyart and D. Quere, *Capillarity and Wetting Phenomena, Drops, Bubbles, Pearls*, Springer, New York, 2003.

25 M. Mionic, S. Jiguet, M. Judelewicz, L. Forro and A. Magrez, *Phys. Status Solidi B*, 2009, 2461–2464.

26 M. Tuller, D. Or and L. M. Dudley, *Water Resour. Res.*, 1999, **35**, 1949–1964.

27 V. Joekar-Niasar, S. M. Hassanizadeh, L. J. Pyrak-Nolte and C. Berentsen, *Water Resour. Res.*, 2009, **45**, W02430, DOI: 10.1029/2007WR006641.